New insights into the protogenic and spectroscopic properties of commercial tannic acid: the role of gallic acid impurities

NJC

Accepted Manuscript

This article can be cited before page numbers have been issued, to do this please use: G. Ghigo, S. Berto, M. Minella, D. Vione, E. Alladio, V. M. M. Nurchi, J. I. I. Lachowicz and P. G. Daniele, *New J. Chem.*, 2018, DOI: 10.1039/C7NJ04903J.

View Article Online
DOI: 10.1039/C7NJ04903J

New Journal of Chemistry

ARTICLE

New insights into the protogenic and spectroscopic properties of commercial tannic acid. The role of gallic acid impurities

Received 00th January 20xx,

G. Ghigo,[a] S. Berto,[a †] M. Minella,[a] D. Vione,[a] E. Alladio,[a] V. M. Nurchi,[b] J. Lachowicz,[b] P. G. Daniele.[a]

Accepted 00th January 20xx

DOI: 10.1039/x0xx00000x

www.rsc.org/

Tannic acid (TA) belongs to hydrolysable tannins, natural polymers derived from the vegetable kingdom. Although TA is described as a molecule with a central core of glucose esterified with five digallic units, its molecular structure has not yet been completely clarified. Actually, TA is described as a mixture of different compounds. In this work, by using potentiometry, UV-vis and fluorescence spectroscopy, as well as *ab initio* calculations we got awareness on protonation properties and spectroscopic features of TA. A preliminary investigation on gallic acid, present as an impurity in the commercial TA mixture, and on methyl 3,4,5-trihydroxybenzoate served as a benchmark for the computational work and to correct the data from the gallic acid contribution. GA principally affects the pH of TA solutions and the fluorescence signals. The data showed the presence of three main types of protogenic groups, with pK_a included in the range of 6-8.5, which can be ascribed to the phenolic functions. The least acidic site shows the highest concentrations, and the dissociation of half of the TA phenolic groups takes place at pH ~ 7.8. The UV-vis spectra of the protonated and deprotonated species were obtained through data elaboration with stoichiometric and chemometric approaches. The results show main absorption maxima (277 and 323 nm, respectively) similar to those obtained with *ab initio* calculations. Overall, we achieved a remarkable coherence among the outcomes obtained by using different methodologies.

Introduction

The molecule of tannic acid (TA) is based on a α/β-D-glucopyranose skeleton whose hydroxyl groups are partially esterified by gallic acid (GA, 3,4,5-trihydroxybenzoic acid). TA belongs to the class of hydrolysable tannins[1,2] that are natural polymers derived from the vegetable kingdom and belonging to the polyphenol family. In the past decade, the attention of the scientific community towards these molecules has increased due to their biological activity as antioxidant agents. In fact, polyphenols can protect the cellular components from oxidative damages by scavenging the harmful Reactive Oxygen Species (ROS)[3,4] and are able to reduce the growth of some fungi, bacteria and viruses.[5-7]

Tannins also occur in surface waters, and they can be used as surrogate of the Natural Organic Matter (NOM). They can simulate the behaviour of relatively hydrophilic compounds with medium molar mass in modelling studies of the water environment.[8,9] Recently the polyphenols, especially those with galloyl groups, have been used in technological processes to prepare coated nanomaterials. Actually, these molecules are versatile surface modifiers with peculiar adhesion properties. In particular polyphenols have been employed to prepare the metal-phenolic networks (MPNs). TA is a suitable coating agent for biointerfaces because of its high biocompatibility and its strong interaction with metal ions, which provides MPNs with additional functionalities.[10,11]

Commercially available TA is sold as a molecule with a 1701.20 g mol^{-1} molecular weight and a structure where the central core of glucose is esterified with five digallic units (Figure 1). However, commercial TA is actually a mixture of gallic acid, methyl gallate, *n*-galloyl glucose and compounds with higher molecular weight, having several gallic units linked together by ester bonds around the glucose core.[12] Despite the hardly defined composition of the commercial mixture called "tannic acid", the latter is used successfully in many application fields

[a] *Università di Torino, Dipartimento di Chimica, Via Pietro Giuria 7, 10125 Torino, Italy.*
[b] *Università di Cagliari, Dipartimento di Scienze Chimiche e Geologiche, Cittadella Universitaria, I-09042 Cagliari, Italy.*
† Corresponding author: silvia.berto@unito.it.
Electronic Supplementary Information (ESI) available: [details of any supplementary information available should be included here]. See DOI: 10.1039/x0xx00000x

View Article Online
DOI: 10.1039/C7NJ04903J

without further purification or separation of the single components.[13-15] Because of the different and interesting properties of these polyphenolic molecules, it could be useful to identify chemical models to properly explain the acid-base properties and the spectral features of the TA mixture. With increasing knowledge of the chemistry of these systems, one can assess their complexation capabilities as well as the interaction with solid substrates or biomolecules. L. Costadinnova *et al*.[16] have studied the acid-base properties of two commercial TA specimens by potentiometry and conductometry. They report a first dissociation constant pK_a = 4.19 for mixtures without gallic acid, and have related this protolysis to the proton of the phenolic group linked to the last galloyl of the chain. In the present work, we studied the protonation models for TA by potentiometry, absorption and fluorescence spectrophotometry, as well as *ab initio* calculations. The work is divided into two parts. In the first one we experimentally revise the acidity and photophysical properties of GA and methylgallate (MG, methyl 3,4,5-trihydroxybenzoate) and improve their assessment (literature already reports several data)[17,18] by comparison with DFT computational data. The goal is both to provide novel information and rationalization of the properties of the two molecules, and to produce a benchmark for the following computational approach. The second part is focused on TA and it is similarly aimed at revising and improving the available experimental data using computational results to rationalise our findings. Moreover, in conjunction with the experimental data, we also aim at improving our knowledge on the TA molecular structure.

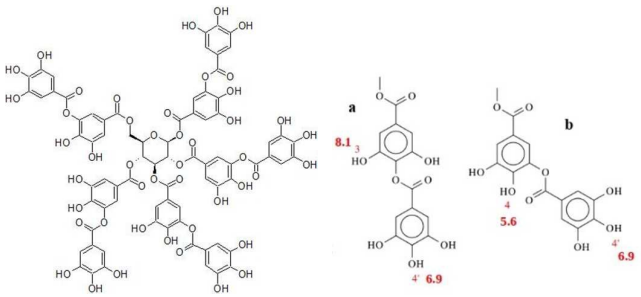

Figure 1 Molecular structure proposed by suppliers for TA; *a* and *b*: molecular structures used as models of the gallic moiety for *ab initio* calculation with the estimated protonation constants (bold red numbers) of phenolic groups in different positions.

Results and discussion

Gallic acid determination

Gallic acid (GA) is the main component of the gallic tannins. The presence of a carboxylic function together with hydroxyl groups allows for the formation of oligomers upon condensation (esterification) between the carboxylic function of a GA molecule and the hydroxyl function of another GA. The carboxylic function can also condensate with the hydroxylic function of a different molecule such as D-glucopyranose, as in the case of TA. Whatever its origin (as unreacted species of the TA synthesis or as product of partial TA hydrolysis), GA can be found in typical commercial TA. Our experiments of hydrolysis carried out on TA solutions in ACN:H_2O with different water contents showed no time evolution at all of the GA concentration (up to 32 h). Therefore, at least at the explored time scale, the hypothesis that GA is formed upon TA hydrolysis seems to be excluded compared to the alternative hypothesis that unreacted GA from the synthesis process still occurs in commercial TA.
We assessed by HPLC the amount of GA occurring in the TA aqueous solutions used in this investigation, and we found it to be non-negligible. GA represents 2,1% of the total TA mass or, on a molar basis by considering the formal TA molecular weight, 19,2% of the molecules occurring in commercial TA. This means that the protons derived from the GA carboxylic function may well affect the acid-base properties of the TA solutions.

Gallic acid (GA) and methyl 3,4,5-trihydroxybenzoate (MG)

pK_a values

The pH-metric titrations of GA and MG solutions were carried out at ionic strength I = 0.1 mol L^{-1} (KCl as ionic medium) and at 25°C. The elaboration of the titration data allowed for the assessment of the protonation constants of these two molecules, and the values thus obtained are reported in Table 1.
We then compared our experimental pK_a values with calculation results, in order to test the accuracy of the computational protocol. To enable comparison with computational data, the experimental protonation constants were extrapolated to null ionic strength by an expanded Debye-Hückel equation[19] (see Table 1).
We assessed the pK_a of GA (dissociation of the carboxylic function) as 4.39 ± 0.01 (I = 0 mol L^{-1}), in quite good agreement with the literature data.[17,20,21] This value is quite well reproduced by the calculations, which yielded a value of 4.7 that is slightly higher than the pK_a value of benzoic acid (4.3[22]) because of the cumulative electronic effects of the three hydroxyl groups of GA. The application of the Hammett's equation[23] leads us to estimate a value of 4.3 for the latter.

View Article Online
DOI: 10.1039/C7NJ04903J

The second and third pK_a values (dissociation of the hydroxyl group in position 4, followed by that in position 3) were, respectively, 8.98 ± 0.01 and 11.73 ± 0.01 (I = 0 mol L^{-1}). These values are not well reproduced by the calculations, because of the difficulties to take into account the stronger and more specific interactions of the di- and tri-anions with the water molecules.

The first and the second pK_a of MG (dissociation of the hydroxyl group in position 4, then in position 3) are, respectively, 7.98 ± 0.01 and 10.59 ± 0.01 (I = 0 mol L^{-1}). Again, the first pK_a value is quite well reproduced by the calculations which yielded a value of 7.8. The acidity of the hydroxyl group in position 4 is quite higher than that of phenol (9.95[24]), because of the cumulative electronic effects of the two *meta* hydroxyl groups and of the methylcarboxylate group. In this case, an estimation of the pK_a through the Hammett's equation[23] is not possible because of the lack of σ parameters for the *ortho* groups.

Because of the distances, we can exclude a role of an intra-molecular hydrogen bond between the vicinal hydroxyl groups (in the calculated structure, the hydroxylic hydrogen atoms are more than 2.2 Å far from the nearest oxygen atom, which is longer than the typical length of a hydrogen bond). The good agreement with the computational results (where the intramolecular hydrogen bond is not present) confirms this conclusion.

Molecule	Experimental values[a] at I = 0.1 mol L^{-1} KCl			Experimental values[a] at I = 0 mol L^{-1}			Calculated values[b]		
	pK^1	pK^2	pK^3	pK^1	pK^2	pK^3	pK^1	pK^2	pK^3
gallic acid	4.20 ± 0.01	8.58 ± 0.01	11.11 ± 0.01	4.39 ± 0.01	8.98 ± 0.01	11.73 ± 0.01	4.7	9.4	17.0
methyl 3,4,5-trihydroxybenzoate	7.78 ± 0.01	10.19 ± 0.01	-	7.98 ± 0.01	10.59 ± 0.01	-	7.8	--	--
tannic acid	6.14 ± 0.01	7.19 ± 0.01	8.39 ± 0.01	6.34 ± 0.01	7.39 ± 0.01	8.59 ± 0.01	5.6	6.9	8.1

Table 1 Protonation constants evaluated by: a) elaboration of pH-metric titrations (experimental values) carried out at ionic strength I = 0.1 mol L^{-1} and at 25°C. The experimental values at I = 0 were calculated upon application of an expanded Debye–Hückel equation.[19] b) For the calculated values see details in the Experimental section and ESI.

Molecule	Experimental values for solution at different pH (nm)		Experimental values for species (nm)		Calculated values (nm)	
	pH 5[a]	pH 9	Phenolic groups protonated[b]	Phenolic group deprotonated[c]	Phenolic groups protonated[b]	Phenolic group deprotonated[c]
gallic acid	259, 212	296, 230sh, 212sh	260, 212	296, 228sh, 212	260, 215, 205	288, 228, 202
methyl 3,4,5-trihydroxybenzoate	272, 216	--	--	--	272, 214	310, 236
tannic acid	275, 214	324, 237	277, 212	323, 278sh, 236, 214sh	282	317

[a] The UV-vis spectra of GA recorded at pH = 5 correspond to the mono-deprotonated form; those of MG and TA at pH = 5 correspond to the neutral molecule. The UV-vis spectra recorded at pH = 9 are mainly due to the species with a deprotonated phenolic group.
[b] For GA the species with the protonated carboxylic function was excluded from the list. Data can be found in the ESI.
[c] The deprotonated species corresponds to the loss of one proton from a phenolic group.

Table 2 UV-vis absorption maxima of: experimental spectra of solutions, experimental spectra of species and calculated spectra. The experimental spectra of species have been obtained by HypSpec® elaboration of the experimental spectra of solutions.

Spectral features

The UV-vis spectra of GA and MG were recorded at pH = 2 and pH = 5, respectively, in order to measure in all cases the absorption spectrum of the neutral molecule. The experimental data were then compared with the calculated ones. For both GA and MG the calculated and experimental spectra were in quite good agreement: GA has absorption maxima at 272 and 211 nm, in comparison with 272 and 213 nm obtained by calculations. Moreover, MG shows maxima at 272 and 216 nm that are comparable with the calculated ones at 272 and 214 nm. The experimental and calculated spectra are reported as raw data and as plots in the electronic supplementary information (here after ESI) file, Tables 1-2_ESI and Figures 1-2_ESI.

The UV-vis spectra of GA, MG and TA were then recorded at higher pH values, in order to measure the absorption spectra of the deprotonated species. The UV-vis spectra of the deprotonated molecules were also computationally simulated: the spectrum of mono-deprotonated GA would show three absorption maxima at 260, 215 and 205 nm, while doubly deprotonated GA would have maxima at 288, 228 and 202 nm. The mono-deprotonated MG species has two calculated maxima at 310 and 236 nm. The experimental and calculated spectra are reported in Figures 1-2_ESI, and the wavelength values of the absorption maxima are summarised in Table 2. In the case of GA it is possible to note a quite good agreement

View Article Online
DOI: 10.1039/C7NJ04903J

between experimental and calculated data also for the anionic species. In contrast, in the case of MG the comparison failed possibly because of the instability of the molecule at alkaline pH. The MG solutions are in fact unstable at pH > 8, and their absorption spectra change during storage (see Figures 3_ ESI). Such behaviour is due to the redox properties of MG, which can be very easily oxidized.[25]

Overall, the agreement between experiments and computation results was quite good for both dissociation constants and absorption spectra, making us confident of a good estimation capability for the TA models (see later).

Because of the non-negligible amount of GA in the TA solutions, UV-vis titrations were carried out on $1 \cdot 10^{-4}$ mol L^{-1} GA at I = 0.1 mol L^{-1} (KCl) and 25°C, in order to evaluate the contribution of GA to the TA absorption spectra. The absorption spectra were elaborated by HypSpec® and the spectrum of the single protonated species was calculated. The absorption maxima of the predominant species in the pH range 5 - 9 were in very good agreement with those calculated by DFT. The mono-deprotonated species shows maxima at 260 and 212 nm, and the di-deprotonated one at 296, ~228 and 212 nm (see Table 2 and Figure 1_ ESI).

The computed GA spectra underwent decomposition with Gaussian functions, and five bands were used to explain the experimental absorbance. The maximum absorbance of each band was plotted as a function of pH (data shown in Figure 5_ESI). The trend of the plot suggests a pK_a value of about 8.7 for the hydroxyl group in position 4, in agreement with the experimental value obtained by potentiometry (8.98±0.01 at I = 0 mol L^{-1}).

Tannic acid

pK_a values

pH-metric titrations were performed on TA solutions and the titration curves thus obtained showed two equivalent points (EP), the first at pH 5.3 and the second at pH 9.5. Between these two EPs there is a wide buffer region (see Figure 2). This behaviour suggests the presence of a relatively acidic function, responsible for the first part of the curve, and a progressive dissociation of the phenolic groups that could reasonably explain the buffer region. After the second EP the data were not taken into consideration because oxidation processes could not be excluded. The experimental data were elaborated with the BSTAC programme[26] by assuming independent deprotonation processes. The presence of GA in the solutions was taken into account during the elaboration procedure. Four types of protogenic functions give a satisfactory portray of the system and can suitably explain the experimental data, as shown in Figure 2a (red curve). The first part of the titration curve can be explained by the carboxylic function of GA and by another species that has a pK_a of 4.15 ± 0.01 (I = 0.1 mol L^{-1}). This species has a low concentration with respect to phenolic functions and could be related to the presence of further carboxylic acids not quantified by HPLC, such as a digallic acid (3,5-dihydroxy-4-(3,4,5-trihydroxybenzoyloxy)benzoic acid, DiGA). Because of the small difference with respect to the first pK_a of GA, an accurate computational estimation of the pK_a of DiGA is not affordable. As an alternative we can estimate the first pK_a by applying the Hammet's equation[23] upon substitution of the GA hydroxyl group occurring in position 4 (σ_p = -0.37) with a benzoyloxy group (σ_p = +0.13). The process causes a reduction of the expected pK_a value, from 4.4 in GA to 3.9 in DiGA. The latter value is close to the experimental one (4.15) and it is coherent with our hypothesis that the above-cited species at low concentration could be DiGA. On the basis of these findings, we can state that the pH of the TA solutions is strongly affected by GA and by other carboxylate species, but that their impact on the total acidity equivalents is low.

The three deprotonation processes reported in Table 1 account for the buffer region of the curves and could be ascribed to the different phenolic functions. On the basis of the proposed speciation model, it is possible to draw a useful species distribution diagram where the phenolic and phenolate percentage is plotted as a function of pH. The sum of the concentrations of the protonated species corresponds to the phenolic fraction, whereas the sum of the concentrations of the deprotonated species was considered as phenolate. The species distribution diagram thus obtained is reported in Figure 2b.

The values of pK_a reported in Table 1 are in quite good agreement with those obtained by *ab initio* calculations on the basis of the structures *a* and *b* shown in Figure 1 (note that the *ab initio* modelling of the whole TA structure is not feasible). Indeed, two intra-molecular H-bonded conformers (a' and b', figure 3b_ESI) have also been identified. In term of free energies, these conformers are respectively located 1.2 and 2.2 kcal mol^{-1} above the structures *a* and *b*. This is possibly because of i) the distortion from the optimal position of the two aromatic moieties (compare figures 3a_ESI and 3b_ESI), ii) the entropy loss (structures a' and b' are more rigid) and iii) the loss of the interaction with water molecules, which would not be compensated by the formation of the intra-molecular H-bonds. Therefore, intra-molecular hydrogen bonds can be neglected for the tested structures.

The theoretical values suggest that the phenolic function of the terminal gallic moiety is more acidic than the internal one, if the ester bond involves the position 4 (see structure *a* of Figure 1). The opposite situation is encountered if the ester bond involves the phenolic group in position 3 (structure *b* of Figure 1). Therefore, three main types of protogenic groups were identified, coherently with the pH-metric model. On the basis of these results, one can think of associating the experimental pK_a values to a specific type of phenolic function, thereby proposing an acid-base model that takes into account the concentration ratios between the different protogenic groups. The elaboration of the experimental data gives defined concentrations of the three protogenic sites as reported in Table 1. In particular, one obtains a molar ratio of about 1:3 for site1:site2, 1:7.5 for site1:site3 and 1:2.5 for site2:site3. In particular, high concentrations were estimated for the least acidic protogenic site (pK_a = 8.59, I = 0 mol L^{-1}). This

View Article Online
DOI: 10.1039/C7NJ04903J

observation could suggest that: i) the ester bond involves preferentially the position 4, and ii) the molecules occurring in solution have a structure that is quite different from that proposed by the usual model (which foresees two units of gallic acid for each chain, Figure 1), in which case the gallic acid chains could be longer than two units.

Spectral features

Spectrophotometric titrations were performed on TA solutions, as reported in the experimental section. The absorption spectra collected as a function of pH are shown in Figure 3 and the absorption maxima are listed in Table 2. We found two different behaviours depending on the pH range considered. Between pH 5 and 9 (Figure 3a) the spectrophotometric evolution is characterised by three well defined isosbestic points at 292, 253 and 225 nm, suggesting the presence of only two species that are differently protonated. The spectrum at pH 5 has two absorption bands, at 275 and 214 nm, and a hump between 275 and 310 nm.

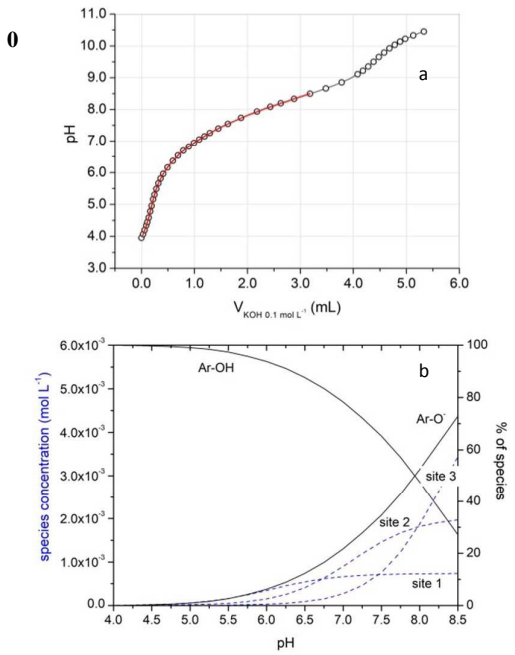

Figure 2 a_ pH metric titration curve of a $1 \cdot 10^{-3}$ mol L^{-1} TA solution in KCl 0.1 mol L^{-1}. Points: experimental data; red line: calculated titration curve obtained with the protonation model reported in Table 1. **b**_Blue dotted lines: concentration of the deprotonated form of the TA protogenic sites (site 1, 2 and 3 have pK_a = 6.14, 7.19 and 8.19, respectively - Table 1), for a nominal concentration of [TA] = $1 \cdot 10^{-3}$ mol L^{-1}, as a function of pH. Black lines: total percentage of protonated and de-protonates sites as a function of pH.

This peak asymmetry was attributed by Arapitsas *et al.*[12] to the ester bonds of the gallic acid chain. By increasing the pH up to 9, the intensity of these bands decreases and two new bands appear with absorption maxima at 324 and 237 nm.

Between pH 9.5 and 11 (Figure 3b) the intensity of the bands at 237 and 324 nm decreases and three new bands appear with absorption maxima at 253, 286 and 400 nm. However, in this pH range the isosbestic points are not well defined and the spectra become quite similar to those obtained with MG at pH > 8.5 (see Figure 3_ESI). Therefore, the spectra recorded at pH ≥ 9 are likely affected by chemical reactions that are different from a simple de-protonation. For this reason, such spectra were not be used for successive elaborations.

Three different approaches were used to elaborate the spectrophotometric data collected between pH 5 and 8.5. The first approach is based on the HypSpec® software to assess the protonation constants and the spectra of the differently protonated species. By so doing we got only one pK_a value (7.53 ± 0.02) and could estimate the spectra of the two species (Figure 3c).

The protonated and deprotonated species show absorption maxima at 277 and 212 nm and at 323, 278sh, 236 and 214sh nm (sh: shoulder), respectively (Table 2). These values are all quite similar to those calculated for the MG species (Figure 2_ESI and Table 2_ESI) and to the main absorption band calculated for the structure *a* shown in Figure 1. The calculated values were in fact 282 and 317 nm for the protonated and the deprotonated form, respectively (data reported in Table 3_ESI). It is reasonable to associate the first spectrum to the protonated form of TA, and the second one to TA having a single phenolate group. Therefore, it is possible to observe that the pK_a value thus obtained is a little lower than that estimated on the basis of the intersection of the curves Ar-OH and Ar-O^- reported in the species distribution diagram (see Figure 2b).

The experimental spectra were then decomposed by using Gaussian functions. Seven bands were used to decompose the spectra, and the heights of the bands were plotted as a function of pH. The plot thus obtained, as well as the positions and the half-widths of the bands are shown in the ESI file (Figure 6_ESI and Table 5_ ESI).

The plots of the main band heights at 326.0, 272.7, 237.4 and 214.9 nm as a function of pH were compared with the species distribution obtained with pK_a = 7.53 (Figure 4). The comparison is satisfactory but the curves do not overlap completely, suggesting a possible contribution of GA to the UV-vis spectra of TA solutions. The estimated pK_a is nonetheless 7.75, a value that is close to that obtained by using potentiometric data.

The spectra were then elaborated through a Multivariate Curve Resolution – Alternating Least Squares (MCR-ALS) approach. More in details, data from spectrophotometric titrations consisted in a 9×251 matrix, corresponding to 9 monitored pH levels (from 5.1 up to 8.7) and 251 wavelengths (from 200 up to 450 nm), for $1.0 \cdot 10^{-5}$ mol L^{-1} TA solutions. Furthermore, non-negativity and closure constraints were employed (*vide infra*). The application of MCR-ALS provided two matrices of optimised estimates of concentration profiles and UV-vis spectra for two species (components) that make up the solutions under investigation. As it can be seen in Figure 7_EIS, the estimated spectra turned very similar to those

View Article Online
DOI: 10.1039/C7NJ04903J

obtained after the use of the HypSpec® software, reported in Figure 3c, thereby supporting the spectrophotometric data interpretation. On the other hand, the concentration profiles from MCR-ALS allowed estimating the pK_a values of the two differently protonated TA species, which turned to be within the range 7.5-7.6 as shown in Figure 8_EIS. This result further supports the previous data.

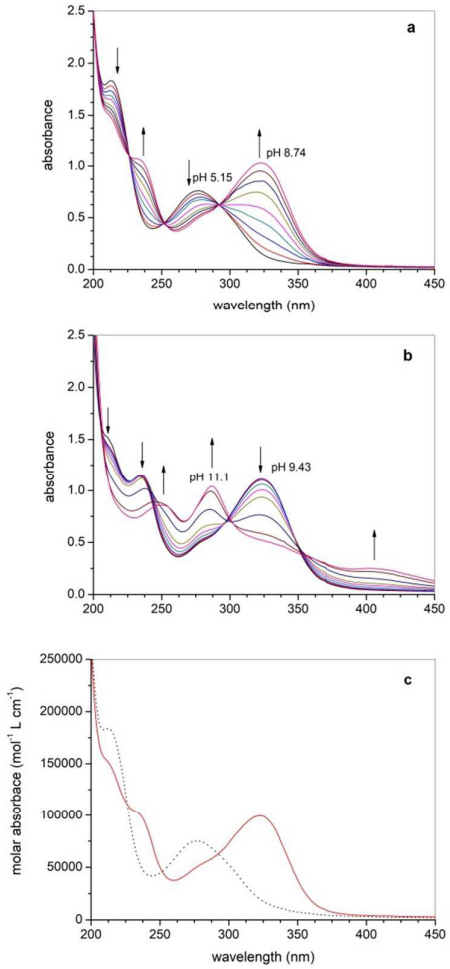

Figure 3 a – b: experimental UV-vis spectra as a function of pH, of a solution containing TA 1 · 10^{-5} mol L^{-1} TA and KCl 0.1 mol L^{-1}. The arrows show the trend of the absorbance as the pH increases. The pH values are the experimental data corresponding to the nearest spectrum. . For readability issues, the overall pH interval was split into two figure panels. **c**: calculated UV-vis spectra of the differently protonated species of TA. Black dotted line: protonated species; red line: deprotonated species.

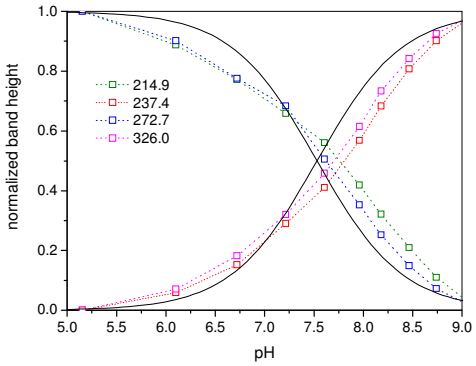

Figure 4 Normalized heights of the bands at 326.0, 272.7, 237.4, 214.9 nm, obtained by decomposition of the 10 spectra between pH 5.15 and 9.17 through the program SpecPeak[27] (points).Speciation plots of tannic acid calculated using a pK_a value of 7.53 (continuous lines).

Fluorescence spectra

The fluorescence excitation–emission matrices (EEM) were recorded on solutions of GA, MG and TA at pH values of about 5 and 9. The contour plots obtained are reported in Figure 5. They show the position of the peaks, characterised by an excitation and an emission wavelength (Ex/Em), and the peak heights by means of a colour scale. The linear features are the first and second harmonic of the Rayleigh–Tyndall scattering and the Raman scattering of water.

At pH 5, where no phenolic dissociation occurs, the emission peaks of GA are at Excitation/Emission wavelengths (Ex/Em) of 210/350 nm and 260/350 nm, those of MG are at 225/367 nm and 270/367 nm, whereas those of TA are at 210/360 and 255/360 nm.

At higher pH, GA shows peaks at 230/420 nm and at 300/375 nm; MG has maxima at 225/380 nm and 320/390 nm, quite similar to those of TA at 225/400 nm and at 325/395 nm. This feature is in agreement with the consistency between the MG and the TA UV-vis spectra at alkaline pH, although the data collected in alkaline conditions were affected by the instability of the phenolate species.

In order to resolve the contribution of GA to the EEM spectra of TA, a MCR-ALS approach was used and non-negativity constraints were selected (see Experimental section and EIS file for details). The evaluated fluorescence data consisted of a column-wise augmented matrix obtained by joining five EEM spectra having 251 excitation wavelengths (from 250 up to 500 nm at steps of 1 nm) and 31 emission wavelengths (from 200 up to 500 nm at steps of 10 nm), i.e. five EEMs of 251×31 size each, resulting into a global dataset of 1255×31 data. The five EEMs corresponded to the GA and the TA fluorescence spectra; in particular, 5.0 · 10^{-6} mol L^{-1} GA solutions were measured at pH 5.0 and 9.0, while 5.0 · 10^{-6} mol L^{-1} TA solutions were measured at pH 5.4, 6.2 and 8.8. In the present case, only non-negativity constraints were selected for both pure spectra and concentration profiles.

MCR-ALS provided useful matrices of optimised estimates of concentration profiles, emission and excitation spectra for four

View Article Online
DOI: 10.1039/C7NJ04903J
Journal Name ARTICLE

species (components) composing the different solutions under investigation.

More in detail, Figure 6 shows the contributions of the four different estimated species to the collected EEM. Due to the fact that the first two samples are GA solutions at pH 5.0 and 9.0, MCR-ALS indicated the presence of two differently protonated GA species that show a complementary contribution to the concentration plot. Then, the MCR-ALS analysis performed on EEM spectra of TA solutions collected at pH 5.4, 6.2 and 8.8 revealed the presence of two differently protonated TA species (as also observed during UV-vis spectra interpretation), together with the previously estimated GA species. Again, the contribution of the evaluated GA and TA species is complementary with reference to the variation of the pH parameter, thus indicating the occurrence of GA contributions to TA when the TA solutions are examined.

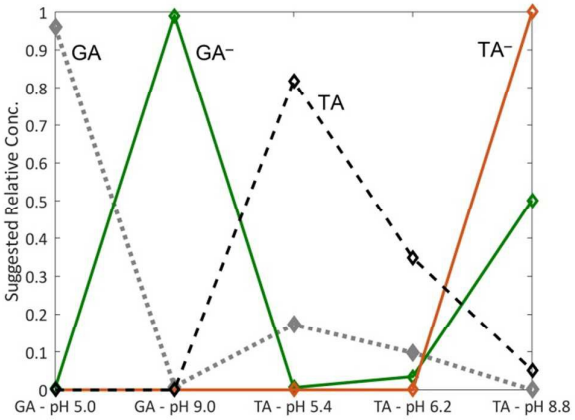

Figure 6 Concentration profiles estimated by MCR-ALS. The x-axis reports the different solutions containing GA and TA measured at different pH levels, while the y-axis shows the relative concentration values suggested by the algorithm (no closure constraints were set). The grey dotted and the black dashed lines represent GA and TA protonated species, respectively, while the green and the red lines stand for the deprotonated GA and TA species, respectively.

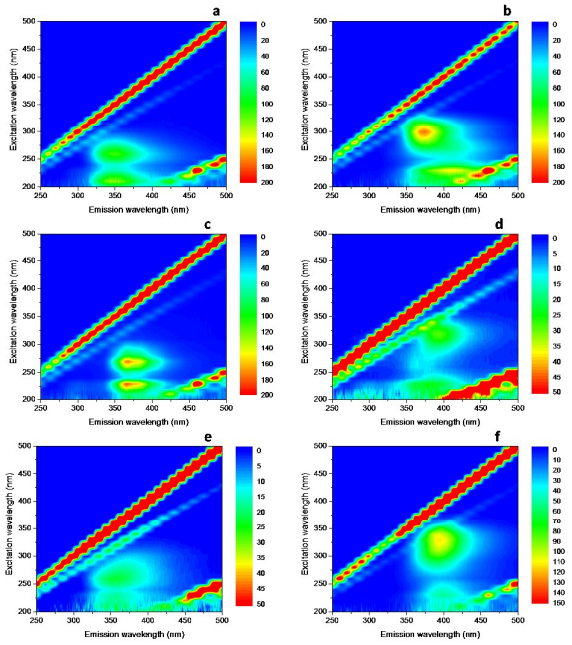

Figure 5 a, b: EEM spectra of a 5.0 · 10^{-6} mol L^{-1} GA solution at pH 5.0 and 9.0; **c, d**: EEM spectra of a 5.0 · 10^{-6} mol L^{-1} MG solution at pH 5.8 and 9.3; **e,f**: EEM spectra of a 5.0 · 10^{-6} mol L^{-1} TA solution at pH 5.4 and 8.8.

In addition, excitation (Figure 9_EIS) and emission spectra (Figure 10_EIS) were estimated by MCR-ALS. The results agree with the contour plots reported in Figure 5. In particular, the excitation spectra (Figure 9_EIS) of the protonated GA species (grey dotted line) showed maximum absorption peaks at the wavelengths of 210 and 260 nm, whereas those of deprotonated GA (green line) were at 225 and 290 nm, similarly to MG. Moreover, MCR-ALS showed two main peaks for the protonated and deprotonated TA species (respectively represented by a black dashed and a red line) at the respective wavelengths of approx. 230 and 340 nm. Finally, wider and less-resolved peaks were observed for the emission spectra estimated by MCR-ALS (Figure 10_EIS). In particular, the GA protonated species (grey dotted line) showed maximum emission at wavelengths around 350 nm, while the GA deprotonated species (green line) showed a maximum at ca. 375 nm. On the other hand, weak estimations were performed for the emission spectra of the TA protonated species (black dashed line), thus confirming the poor signals measured with the TA solution at pH 5.4. Finally, a maximum emission peak was found for the deprotonated TA species (red line) at wavelengths around 400 nm, thus confirming once again the visual interpretation of the EEM contour plots reported in Figure 5.

View Article Online
DOI: 10.1039/C7NJ04903J

Experimental

Chemicals

Gallic acid (GA, >98%), tannic acid (TA, puriss.) and acetonitrile (99.9%, HPLC gradient grade) were from Sigma Aldrich (St. Louis, Missouri, USA). Methyl 3,4,5-trihydroxybenzoate (MG, 99%) was from Acros Organics (Geel, Belgium). Potassium hydroxide and hydrochloric acid solutions used as titrant, or for adjusting pH, were prepared by diluting Merck (Darmstadt, Germany) concentrated products. Ultrapure water (Milli-Q, Millipore) was used to prepare all the solutions. The concentration of the potassium hydroxide solution was assessed by standardisation against potassium hydrogen phthalate (Sigma-Aldrich). The purity and the title of the used acids were evaluated by pH-metric titrations.

Apparatus

A Metrohm potentiometer (model 713, resolution of ±0.1 mV) and the titrator Titrando 888 (resolution of ±0.1 mV) were used for pH-metric titrations. They were coupled with Metrohm 765 Dosimat burettes (minimum deliverable volume of ±0.001 cm^3) and equipped with Metrohm combined glass electrodes (mod. 6.0259.100). The temperature of the solutions was controlled by a thermocryostat (mod. D1-G Haake, Victoria, Australia).

The absorption spectra were recorded with a Jasco V-550 UV–vis double-beam spectrophotometer, equipped with Hellma quartz cuvettes (1.000 cm optical path length).

A Varian Cary Eclipse fluorescence spectrofluorometer was used to record the fluorescence excitation–emission matrix (EEM) spectra with Helma cuvettes (1.000 cm × 1.000 cm optical path lengths).

The quantification of the GA impurities in commercial TA was carried out through a YL HPLC system 9300, equipped with a YL9330 Column Compartment thermostated at 35 °C and a YL9150 autosampler. The employed column was a RP C18 LiChroCART® (125×4mm) with 5 μm LiChrosphere® particles.

Procedures

The titrator Titrando 888 was used in DET (Dynamic Equivalence point Titration) modality and the maximum accepted signal drift was 0.05 mV min^{-1}. Measurements were carried out at 25 ± 0.1 °C.

The electrode couple was daily calibrated in terms of H^+ concentration by titrating a 5 $\cdot 10^{-3}$ mol L^{-1} HCl solution at the working ionic strength (0.1 mol L^{-1}) with standard KOH. In this way we could assess the slope and the formal potential E^0 of the Nernst equation. In order to avoid O_2 and CO_2 contamination during the titration, a stream of purified N_2 was bubbled in the titration cell.

The titrations were carried out on solutions with ionic strength of 0.1 mol L^{-1}, and KCl was used as ionic medium. Therefore, 50 mL of solutions of GA or MG, with concentrations included between $1.0 \cdot 10^{-3}$ and $2.0 \cdot 10^{-3}$ mol L^{-1}, were titrated with 0.1 mol L^{-1} KOH in order to evaluate the protonation constants of the relevant compounds. The same procedure was also used for TA solutions with nominal concentrations included between $0.5 \cdot 10^{-3}$ and $2.0 \cdot 10^{-3}$ mol L^{-1}.

The UV-vis spectra were recorded in the range of 200-450 nm, and a baseline was taken in air before each absorbance measurement. Each absorbance spectrum was taken against the reference cuvette filled with Milli-Q water or with KCl 0.1 mol L^{-1}. Spectrophotometric titrations were performed on solutions with: (i) nominal TA concentrations of $0.5 \cdot 10^{-5}$ and $1.0 \cdot 10^{-5}$ mol L^{-1}, in KCl 0.1 mol L^{-1}, and (ii) a GA concentration of $1.0 \cdot 10^{-5}$ mol L^{-1}, in KCl 0.1 mol L^{-1}. The temperature was maintained at 25°C, and the pH was measured with the apparatus mentioned before.

The fluorescence excitation–emission matrices (EEM) were taken with excitation wavelengths in the range of 200 – 500 nm, at 10 nm intervals, and emission wavelengths from 250 to 500 nm. A 10 nm bandpass was adopted on both excitation and emission. The pH of the solutions was adjusted with KOH. The Raman signal of water was taken as a reference for signal stability within different measurements.

The HPLC determinations were carried out in isocratic mode at 1 mL min^{-1} with H_3PO_4 $4.2 \cdot 10^{-3}$ mol L^{-1}: acetonitrile 97:3. The retention time of GA was 4.2 min. The detection was carried out at 272 nm and the volume of injection was 50 μL. The hydrolysis kinetics of TA to give GA was evaluated by measuring the time evolution of the GA concentration (up to 32 h), in water/acetonitrile (ACN) mixtures with different concentrations of water (from 0 to 100 %). The determination of the concentration of GA in TA solutions, with both water and H_2O:ACN at different ratios as solvents, was carried out by calibrating the analytical response with GA standard solutions prepared in the same solvents used for the hydrolysis experiments.

Data elaboration

The electrode calibration data were elaborated by the ESAB2M program[28] in order to refine the electrode parameters: formal potential E^0, Nernstian slope and analytical concentration of reagents. The BSTAC program[26] was used for the elaboration of the titration points of each investigated system, in order to evaluate the protonation constants.

The UV-vis spectra were elaborated with different approaches in order to evaluate the protonation constants and the molar absorptivity of the protonated species with independent techniques. HypSpec® software[29] was used first. It works with stoichiometric principles by applying mass balance equations

View Article Online
DOI: 10.1039/C7NJ04903J

and Lambert-Beer's law. A decomposition of the spectra with Gaussian functions was also employed, and the trend of the maximum peaks was plotted as a function of pH in order to achieve a pK_a estimation. Finally, data were elaborated by Multivariate Curve Resolution – Alternating Least Squares (MCR-ALS), a chemometric technique that identifies the main sources of variability of a specific dataset without any a-priori knowledge about the analytes contributing to the measured signals.[30]

In the present study, the preliminary un-mixing procedure was carried out using the variable "purity" approach with allowed noise parameter of 10%. Finally, once carried out the preliminary estimations, the MCR-ALS optimisation process starts up to the achievement of convergence. The latter can be monitored through the evaluation of parameters like, for instance, the explained percentage variance (EV%) and the lack-of-fit (%LOF).[31,32] More in details, optimisation stops when the difference between two fitted models obtained after two consecutive iterations is no longer significant, so that no improvement is obtained. Conditions such as the non-negativity, the unimodality, the equality and the closure of the concentration profiles and the pure spectra, may be selected by pre-defined constraints. The adoption of constraints is fundamental since they allow obtaining unique solutions by decreasing the scalar and rotational uncertainties for both the estimated concentration profiles and their spectra. In the present study, a non-negativity constraint was carried out by means of fast non-negative least squares algorithm (fnnl).[33] Closure constraints, whenever applied to concentration profiles, were set to 1. MCR-ALS analysis was performed using the GUI code developed by Jaumot *et al.*[31,32] for MATLAB environment, freely downloadable at http://www.mcrals.info/ (MATLAB version R2017b was used).[34]

The computational study was performed within the Density Functional Theory (DFT).[35-37] Bulk solvent effects (water) to the electronic energies were introduced in all calculations by the Polarized Continuum Method (PCM)[38,39] within the universal Solvation Model Density.[40] As functional we used the functional PBE0[41,42] in combination with the Pople's basis set 6-311+G(d,p).[43,44]

The exact calculation of the pK_a of an acid is quite a though challenge.[45] Here, the deprotonation equilibria were modelled with the same fruitful approach used in a previous work,[46] that allowed getting a good agreement with the calculated and experimental phenol pK_a. The method consisted in the calculation of the free energy of proton transfer from a complex of the acid AH with water to a tetramer of water:

$$[AH\,(H_2O)_n] + (H_2O)_4 \leftrightarrows [A\,(H_2O)_n]^- + [H_3O\,(H_2O)_3]^+$$

The absorption spectra were obtained with single-point Time-Dependent DFT (TD-DFT)[47,48] by calculations on the geometries of the neutral and dissociated anion, without explicit water molecules. This method provides a reasonable accuracy at reasonable computational costs (time and computing resources).[49,50] The calculated absorption spectra were obtained through linear combination of gaussian functions centred on the calculated electronic transition frequencies, with relative height calculated from the oscillator strength as explained in the literature.[51,52] For the GA and MG neutral species, the best agreement with the experimental findings was obtained without explicit water molecules. For their corresponding dissociated anion species, some explicit water molecules were required. On the basis of the methodological deductions from the cases of GA and MG, the same approach was used for the TA models.

Calculations were performed using the quantum package Gaussian 09-A.[53] The pictures of structures in Figures 1-4 in the ESI were obtained with the graphical program Molden.[54]

Conclusions

Combining potentiometry, UV-vis and fluorescence spectroscopy, as well as *ab initio* calculations, a deeper understanding was achieved of the protogenic and spectroscopic properties of commercial tannic acid. Both pH-metric titrations and theoretical data highlight the occurrence of three main types of protogenic groups assigned to different positions of the phenolic functions in the gallic acid chain. The pK_a of the protogenic sites are included in the 6-8.5 interval, and the concentration of the less acidic site is quite higher than the others. Because of the carboxylic function, the presence of significant GA impurities in commercial TA affects considerably the pH of the TA solutions. In contrast, the impact of GA is quite low on the total acidity equivalents of TA.

The spectroscopic data recorded on TA solutions show the signals of two species assigned to protonated and deprotonated TA, in agreement with the theoretical simulations. The elaboration of UV-vis data, by both stoichiometric and chemometric approaches, gave us the pK_a value and the spectra of the single species. The results thus obtained are in quite good agreement with the protonation constants derived by potentiometry, when assuming that the different deprotonated forms cannot be differentiated by spectrophotometric techniques. In fact, the pK_a of 7.5 estimated in this way agrees well with the species distribution, obtained with the protonation model proposed on the basis of pH-metric data. In that model, the deprotonated forms were jointly represented (Figure 2_b; continuous black lines).

Overall, we can state that GA impurities occurring in commercial TA play a key role in the fluorescence properties of TA itself, and largely determine the pH values of TA solutions. Moreover, the Multivariate Curve Resolution – Alternating Least Squares (MCR-ALS) technique turned out to be useful in the interpretation of the spectroscopic data and, in particular, to differentiate the contribution of GA on the fluorescence spectra of TA. The approach here proposed for the investigation of the TA protogenic and spectroscopic features could be stimulating for further studies, both into the complexation capability of TA toward naturally occurring or human released metallic cations, and into the understanding of NOM fluorescence.

View Article Online
DOI: 10.1039/C7NJ04903J

Conflicts of interest

There are no conflicts to declare.

Acknowledgements

SB and VMN acknowledge support by MIUR-PRIN 2015 - 2015MP34H3_002. GG acknowledges support by University of Torino, Local founding GHIG_RILO_16_02.

Notes and references

1 M. J. C. Rhodes, *Proceedings of the Nutrition Society*, 1996, **55**, 371
2 R. V. Barbehenn and C. P. Constabel, *Phytochemistry*, 2011, **72**, 1551.
3 S. Caillet, S. Salmieri and M. Lacroixand, *Food Chemistry*, 2006, **95**, 1.
4 Q. Shaikh, M. Yang, K. Memon, M. Lateef, D. Na, S. Wan and T .Jiang *Carbohydrate Research*, 2016, **430**, 72, DOI: 10.1016/j.carres.2016.04.021
5 K. T. Chung, T.Y. Wong, Ch. Wei, Y.W. Huang and Y. Lin, *Critical Reviews in Food Science and Nutrition,* 1998, **38**, 421;
6 G. Liu, S. Xiong, Y. F. Xiang, C. W. Guo, F. Ge, C. R. Yang and K. Kitazato, *Archives of Virology*, 2011, **156**, 1359, DOI: 0.1007/s00705-011-0989-9
7 X. Liu, A. Malki, Y. Cao, Y. Li, Y. Qian, X. Wang and X. Chen, *Experimental and Clinical Endocrinology and Diabetes*, 2015, **123**, 308, DOI: 10.1055/s-0035-1548789.
8 W. Stumm and J. Morgan, Aquatic Chemistry, 2nd ed., Wiley, New York, 1981.
9 K. V. Plakas and A. J. Karabelas, *Journal of Membrane Science*, 2009, **336**, 86.
10 H. Ejima, J.J. Richardson and F. Caruso, *Nano Today*, 2017, **12**, 136.
11 J. Guo, Y. Ping, H. Ejima, K. Alt, M. Meissner, J. J. Richardson, Y. Yan, K. Peter, D. von Elverfeldt, C. E. Hagemeyer and F. Caruso, *Angewandte Chemie International Edition*, 2014, **53**, 5546.
12 P. Arapitsas, S. Menichetti, F. F. Vincieri and A. Romani, *Journal of Agricultural and Food Chemistry*, 2007, **55**, 48.
13 M. G. Albu, M. V. Ghica, M. Giurginca, V. Trandafir, L. Popa and C. Cotrut, *Revista de Chimie*, 2009, **60**, 666.
14 H. Ejima, J. J. Richardson, K. Liang, J. P. Best, M. P. van Koeverden, G. K. Such, J. Cui and F. Caruso, *Science*, 2013, **341** 154.
15 I. Gülcin¸ Z. Huyut, M. Elmastaş and H. Y. Aboul-Enein, *Arabian Journal of Chemistry*, 2010, **3**, 43.
16 L. Costadinnova, M. Hristova, T. Kolusheva and N. Stoilova, *Journal of the University of Chemical Technology and Metallurgy*, 2012, **47**, 3, 289.
17 H. K. J. Powell and M.C. Taylor, *Australian Journal of Chemistry*, 1982, **35**, 739;
18 S. V. Jovanovic, M. G. Simic, S. Steenken and Y. Hara, *Journal of the Chemical Society, Perkin Transactions 2*, 1998, 2365.
19 A. Casale, P. G. Daniele, A. De Robertis and S. Sammartano, *Annali di Chimica (Rome)*, 1988, **78**, 249.
20 B. Sandmann, M C. Hien and R. Sandmann; *Analytical Letters*, 1985, **18**, 149.
21 L. Loginova, V. Medyntsev and B. I. Khomutov, *Zhurnal Obshchei Khimii*, 1972, **42**, 4, 739.
22 H. Gampp, M. Maeder, A. Zuberbuhler and T. Kaden, Talanta, 1980, **27**, 513.
23 C. Hansch, A. Leo and R. W. Taft, *Chemical Reviews*, 1991, **91**, 165.
24 D. R. Lide, CRC Handbook of Chemistry and Physics, 83rd ed. Boca Raton, Fl: CRC Press Inc., 2002-2003, 8-49.
25 M. Asnaashari, R. Farhoosh and A. Sharif, *Food Chemistry*, 2014, **159**, 439.
26 C. De Stefano, P. Mineo, C. Rigano and S. Sammartano, *Annali di Chimica*, 1993, **83**, 243.
27 M. Arca, M. C. Aragoni, G. Crisponi and V. M. Nurchi, *Analytica Chimica Acta*, 1995, **316**, 195.
28 C. De Stefano, P. Princi, C. Rigano and S. Sammartano, *Annali di Chimica (Rome)*, 1987, **77**, 643.
29 P. Gans, A. Sabatini and A. Vacca, *Talanta*, 1996, **43**, 1739.
30 A. de Juan, J. Jaumot and R. Tauler, *Analytical Methods*, 2014, **6**, 4964.
31 J. Jaumot, R. Gargallo, A. De Juan and R. Tauler, *Chemometrics and Intelligent Laboratory Systems*, 2005, **76**, 101.
32 J. Jaumot, A. de Juan and R. Tauler, *Chemometrics and Intelligent Laboratory Systems*, 2015, **140**, 1.
33 R. Bro and S. De Jong, *Journal of Chemometrics*, 1997, **11**, 393.
34 MATLAB Release 2012b, The MathWorks, Inc., Natick, Massachusetts, United States.
35 F. Jensen, Introduction to Computational Chemistry, John Wiley & Sons, NY, 1999, ISBN 0-471-98425-98426.
36 R.G. Parr and W. Yang, Density Functional Theory of Atoms and Molecules, Oxford University Press, 1989.
37 W. Kohn, A.D. Becke and R.G. Parr, *Journal of Physical Chemistry*, 1996, **100**, 12974.
38 B. Mennucci and J. Tomasi, *The Journal of Chemical Physics*, 1997, **106**, 5151.
39 M. Cossi, N. Rega, G. Scalmani and V. Barone, *The Journal of Chemical Physics*, 2001, **114**, 5691.
40 A. V. Marenich, C. J. Cramer and D. G. Truhlar, *The Journal of Chemical Physics B*, 2009, **113**, 6378; A. V. Marenich, C. J. Cramer and D. G. Truhlar, *The Journal of Chemical Physics B*, 2009, **113**, 4538.
41 J. P. Perdew, K. Burke and M. Ernzerhof, *Physical Review Letters*, 1996**, 77**, 3865; J. P. Perdew, K. Burke and M. Ernzerhof, *Physical Review Letters*, 1997, **78**, 1396.
42 C. Adamo and V. Barone, *The Journal of Chemical Physics*, 1999, **110**, 6158.
43 A. D. McLean and G. S. Chandler, *The Journal of Chemical Physics,* 1980, **72**, 5639.

View Article Online
DOI: 10.1039/C7NJ04903J

44 T. Clark, J. Chandrasekhar, G. W. Spitznagel and P. V. R. Schleyer, *Journal of Computational Chemistry*, 1983, **4**, 294.

45 T. Matsui, T. Baba, K. Kamiyad and Y. Shigetab, *Physical Chemistry Chemical Physics*, 2012, **14**, 4181.

46 F. Barsotti, G. Ghigo, S. Berto and D. Vione, *Photochemistry Photobiology Science*, 2017, **16**, 527.

47 R. Bauernschmitt and R. Ahlrichs, *Chemical Physics Letters*, 1996, **256**, 254.

48 A. Dreuw and M. Head-Gordon, *Chemistry Review*, 2005, **105**, 4009.M-35, 36.

49 D. Jacquemin, E. A. Perpète, O. A. Vydrov, G. E. Scuseria and C. Adamo, *The Journal of Chemical Physics,* 2007, **127**, 094102.

50 D. Jacquemin, V. Wathelet, E. A. Perpète and C. Adamo, *Journal of Chemical Theory and Computation*, 2009, **5**, 2420.

51 Gaussian Web site, page: http://www.gaussian.com/g_whitepap/tn_uvvisplot.htm, consulted 13 June 2016.

52 P. J. Stephens and N. Harada, *Chirality*, 2010, **22**, 229-233.

53 M. J. Frisch, G. W. Trucks, H. B. Schlegel, G. E. Scuseria, M. A. Robb, J. R. Cheeseman, G. Scalmani, V. Barone, B. Mennucci, G. A. Petersson, H. Nakatsuji, M. Caricato, X. Li, H. P. Hratchian, A. F. Izmaylov, J. Bloino, G. Zheng, J. L. Sonnenberg, M. Hada, M. Ehara, K. Toyota, R. Fukuda, J. Hasegawa, M. Ishida, T. Nakajima, Y. Honda, O. Kitao, H. Nakai, T. Vreven, J. A. Montgomery Jr., J. E. Peralta, F. Ogliaro, M. Bearpark, J. J. Heyd, E. Brothers, K. N. Kudin, V. N. Staroverov, R. Kobayashi, J. Normand, K. Raghavachari, A. Rendell, J. C. Burant, S. S. Iyengar, J. Tomasi, M. Cossi, N. Rega, J. M. Millam, M. Klene, J. E. Knox, J. B. Cross, V. Bakken, C. Adamo, J. Jaramillo, R. Gomperts, R. E. Stratmann, O. Yazyev, A. J. Austin, R. Cammi, C. Pomelli, J. W. Ochterski, R. L. Martin, K. Morokuma, V. G. Zakrzewski, G. A. Voth, P. Salvador, J. J. Dannenberg, S. Dapprich, A. D. Daniels, Ö. Farkas, J. B. Foresman, J. V. Ortiz, J. Cioslowski, D. J. Fox, Gaussian 09, Gaussian, Inc., Wallingford, CT, 2009.

54 G. Schaftenaar and J. H. Noordik, *Journal of Computer-Aided Molecular Design*, 2000, **14**, 123.

View Article Online
DOI: 10.1039/C7NJ04903J

Table of contents entry

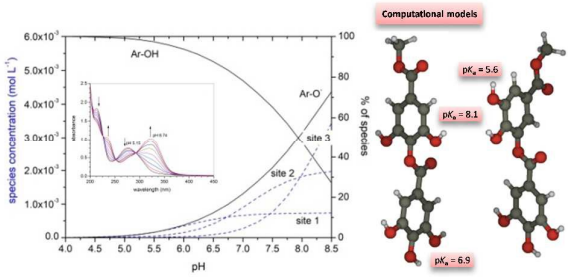

Assessment of a protonation model for tannic acid and characterization of the spectral features of its protonated and dissociated species